

High resolution electron scattering from high spin states in ^{208}Pb

J. P. Connelly,* D. J. DeAngelis, J. H. Heisenberg, F. W. Hersman, W. Kim, M. Leuschner,
T. E. Milliman, and J. Wise†

Department of Physics, University of New Hampshire, Durham, New Hampshire 03824

C. N. Papanicolas

Department of Physics and Nuclear Physics Laboratory, University of Illinois, 1110 West Green Street, Urbana, Illinois 61801

(Received 2 March 1992)

Inelastic electron scattering cross sections have been measured from high spin transitions in ^{208}Pb . Measurements were made over a range of momentum transfer of 1.1 to 2.9 fm^{-1} with energy resolution between 14 and 22 keV. In addition to the previously measured 14^- , 12^- , and 12^+ levels, electron scattering cross sections have been measured on $M11$, $M10$, $M9$, $E9$, and $E7$ transitions. High spin states are quenched from the predicted Woods-Saxon single particle amplitudes by 22% to 67%. Evidence is presented for the fragmentation of the 7.06 MeV 12^- transition strength. Results are interpreted in terms of the independent particle model.

PACS number(s): 25.30.Dh, 27.80.+w

I. INTRODUCTION

The ^{208}Pb nucleus has been the subject of much experimental and theoretical interest. Being the heaviest stable nucleus with both closed neutron and proton shells, ^{208}Pb is simply the best testing ground for available microscopic structure predictions based upon mean-field calculations. In particular, the investigation of high spin transitions in ^{208}Pb has been fruitful. Since the number of contributing configurations are constrained by the selection rules governing angular momentum coupling, high spin transitions in ^{208}Pb are built upon a small number of one-particle-one-hole (1p-1h) excitations. In the extreme single particle model, for instance, the $M14$ (6.745 MeV) and $E12$ (6.110 MeV) transitions will be entirely due to a single 1p-1h excitation.

In the same approximation, magnetic transitions in the excitation region between 5 and 7.2 MeV with $J = 12, 11$, and 10 are limited to two 1p-1h configurations with single particle energies below 7.2 MeV. Lallena [1] has shown that mixing between the $\nu(1j_{15/2}, 1i_{13/2}^{-1})$ and $\pi(1i_{13/2}, 1h_{11/2}^{-1})$ configurations influences the relative strengths of the 6.37 and 7.06 MeV $M12$ transitions seen in electron and proton scattering. The contribution of the less dominant configuration in the $M12$ transitions, however, was shown to be only a few percent. This is to be expected. The residual interaction for magnetic transitions is weak and slightly repulsive; collectivity does not build and the transitions are dominated by a single particle-hole configuration.

The simplicity of the structure of the high spin states

permits the investigation of deviations from standard mean-field theories. Several high spin states (12^+ , 6.10 MeV; 12^- , 6.43 and 7.06 MeV; 14^- , 6.75 MeV) have been identified in earlier (e, e') [2,3] and (p, p') [4–6] experiments. An important result from all of these measurements is the quenching of the single particle-hole amplitudes. The observed cross sections from these states in (e, e') and (p, p') experiments are reported to be approximately 50% of the single particle-hole predictions.

Several mechanisms have been suggested to explain the source of this quenching. Core polarization contributions through a δ residual interaction have been investigated by Hamamoto, Lichtenstadt, and Bertsch [7] and Suzuki *et al.* [8] using a G -matrix interaction. Krewald and Speth *et al.* [9] have suggested that inclusion of 2p-2h contributions fragments the single particle strength. An analysis of not only the very high spin states, but of levels with a lower multipolarity but still dominated by a single 1p-1h excitation, is desirable in the evaluation of the contributions from these various effects. Pandharipande, Papanicolas, and Wambach [10–12] argue that most of the quenching observed for these transitions is derived from the fractional occupancy of the shell-model orbitals involved. The origin of this quenching is attributed to short- and long-range correlations which are not properly accounted for in mean-field theories. Within this interpretation, the measured quenching factors provide a very good measure of occupation numbers which are found to be in excellent agreement with those expected from many-body theory.

This experiment was prompted by the improvement in energy resolution in the high resolution spectrometer at the Bates-MIT electron accelerator to better than $8 \times 10^{-5} \Delta p/p$. The increased energy resolution, improved by a factor of 2 over previous electron scattering experiments on ^{208}Pb , permitted a cleaner measurement of closely spaced levels and provided a more precise determination of the excitation energies and the quenching factors. Our goals were to confirm or improve the re-

*Present address: Physics Department, Hannan Hall, Catholic University of America, Washington, D.C. 20064.

†Present address: Nuclear Physics Laboratory, University of Colorado, Boulder, Colorado 80309-0390.

sults given in previous measurements on the known high spin states, and to identify and analyze the other members of multiplets resulting from the same particle-hole configurations as the known high spin states. The measurement of low-multipolarity, negative-parity states in ^{208}Pb will be presented in a forthcoming publication.

II. ELECTRON SCATTERING

Derivations of the plane-wave Born approximation (PWBA) and the distorted-wave Born approximation (DWBA) are given in many references [13–19] and we will present only the relevant formalism. In the PWBA, the electron scattering cross section is given by

$$\frac{d\sigma}{d\Omega} = \sigma_{\text{Mott}} \eta Z^2 \left\{ \sum_{L \geq 0} |F_L^C(q)|^2 + \left[\frac{1}{2} + \tan^2 \frac{\theta}{2} \right] \times \sum_{L \geq 1} [|F_L^E(q)|^2 + F_L^M(q)^2] \right\}, \quad (1)$$

where the density of final states η is given by

$$\eta = \left[1 + \frac{2E_i}{Mc^2} \sin^2(\theta/2) \right]^{-1} \quad (2)$$

and

$$\sigma_{\text{Mott}} = \frac{\pi \alpha^2}{E_i^2 \sin^4(\theta/2)} \cos^2(\theta/2) \quad (3)$$

is the cross section derived from electrons scattering off a point charge, and

$$q^2 = \frac{4E_i E_f}{\hbar^2 c^2} \sin^2(\theta/2), \quad (4)$$

where q is the momentum transfer.

To first order, the distortion of the electron wave by the Coulomb field of the nucleus may be partially corrected by the use of an effective momentum transfer,

$$q_{\text{eff}} = q \left[1 + \frac{4}{3} \frac{Z \alpha \hbar c}{E_i R_{\text{rms}}} \right]. \quad (5)$$

The effective momentum transfer provides a better estimate of the momentum actually transferred to the nucleus and will be used for the purpose of displaying the experimental form factors.

The nuclear structure information is contained entirely in the Coulomb form factor $F_L^C(q)$ and the transverse form factors F_L^E and F_L^M . Since the contribution of the transverse form factors to the total cross section has an angular dependence of $\frac{1}{2} + \tan^2(\theta/2)$, the transverse and longitudinal components may be separated by measuring the cross section at different scattering angles but at the same momentum transfer. The measurement of the electron scattering cross section at backward scattering angles increases the ratio of the transverse to longitudinal form factor. Magnetic transitions are entirely transverse

and are best measured at a backward scattering angle; the forward angle data are used to verify that the transition is transverse in character.

For large- Z nuclei such as ^{208}Pb , the distortion of the electron wave function from the Coulomb field of the nucleus must be included in any realistic calculation. The DWBA calculations were performed using the programs FOUDES1, FOUDES2, and FOUDES2A [18].

In the analysis of the high spin states, DWBA fits to the data were performed using a linear superposition of Woods-Saxon (WS) wave functions to describe the radial transition densities. The analysis was performed by adjusting the overall amplitude of the particle-hole configuration and the WS radial parameters. The binding energies of the single particle wave functions were taken from Ref. [20].

The transition current densities are the result of both the convective current and the magnetization of the nucleons. Following Ref. [17], these densities are expressed in the single particle model as

$$J_{\lambda, \lambda+1}^{ab, C} = \frac{\hbar}{2mc} C_{ab, \lambda} \frac{1}{\sqrt{\lambda+1}\lambda} \times \left\{ (\lambda+1) \left[\frac{du_a}{dr} u_b - u_a \frac{du_b}{dr} \right] + [l_b(l_b+1)] - [l_a(l_a+1)] \frac{u_a u_b}{r} \right\}, \quad (6)$$

$$J_{\lambda, \lambda+1}^{ab, M} = \mu \frac{\hbar}{2mc} C_{ab, \lambda} \frac{1}{\sqrt{\lambda+1}\lambda} (\chi_b - \chi_a) \times \left[\frac{d}{dr} - \frac{\lambda}{r} \right] u_b u_a, \quad (7)$$

$$J_{\lambda, \lambda}^{ab, M} = \mu \frac{\hbar}{2mc} C_{ab, \lambda} \frac{1}{\sqrt{\lambda}\lambda} (\chi_b - \chi_a) \times \left[\frac{d}{dr} - \frac{\lambda+1}{r} \right] u_b u_a, \quad (8)$$

where u_i are the single particle wave functions, $\chi = (l-j)(2j+1)$ and μ is the magnetic moment of the nucleon participating in the excitation. The spectroscopic factors, $C_{ab, \lambda}$ are given by

$$C_{ab, \lambda} = (-1)^{j_a - 1/2} \frac{\hat{j}_a \hat{j}_b \hat{\lambda}}{(4\pi)^{1/2} \hat{j}_f} \begin{bmatrix} j_a & j_b & \lambda \\ \frac{1}{2} & -\frac{1}{2} & 0 \end{bmatrix}.$$

The form of the Wigner-Eckart theorem used [17] gives $C_{ab, \lambda} = 1$ for pure single particle transitions.

To be compared to the experimental data, the densities given above must be corrected for the finite size of the nucleons. The WS densities were folded with the proton charge distribution using the proton charge form factor taken from Ref. [21]. The magnitude of the neutron charge form factor is small enough to be ignored. The fitted transition densities were transformed into momentum transfer space and compared to the experimental data as form factors.

The single particle wave functions u_i were calculated from a Woods-Saxon potential with a spin-orbit coupling.

The adjustable parameters in the potential were the radius and well depth (taken to be independent for each orbital); the spin-orbit coupling $V_{s.o.}$ and the well-diffuseness parameter $A_{s.o.}$ were fixed ($V_{s.o.}=7.5$ MeV, $A_{s.o.}=0.7$ fm). The amplitude for each particle-hole excitation was varied in the least-squares fit to the cross sections. The well depth for each orbit was taken to be the value producing the correct experimentally observed separation energies.

III. EXPERIMENTAL ARRANGEMENT

Data for this experiment were taken at the MIT-Bates Linear Accelerator Center. The accelerator, spectrometer, and focal plane detection system have been fully described elsewhere [22,23] and only a brief summary will be included here. Electrons with beam energies ranging from 100 to 300 MeV were incident on isotopically enriched ^{208}Pb targets and detected with the 900 MeV Energy Loss Spectrometer (ELSSY). A $\pm 0.3\%$ momentum dispersed beam was focused on the target to match that of ELSSY. The maximum solid angle, defined by movable slits at the entrance of the spectrometer, was 3.325 msr.

Twelve thin 99.86% isotopically enriched ^{208}Pb targets were used for this experiment. Target thicknesses ranged from 2.5 to 4.0 mg/cm². Although average beam currents of up to 60 μA were available, due to target considerations the average current was kept below 25 μA . The beam current was measured to one part in 10^3 by two nonintercepting toroids. A beam energy calibration was performed by measuring the differential recoil between ^9Be , ^{16}O , ^{92}Mo , and ^{208}Pb .

A total of 12 forward angle measurements were taken between 40° and 110° with electron energies from 150 to 300 MeV. Seven measurements at 155° were taken with energies ranging from 100 to 250 MeV. The energy resolution for data reconstructed off line ranged from 12 to 18

keV for the forward angle spectra and from 16 to 24 keV at the backward scattering angle. Figure 1 shows a sample spectrum ($E_0=279$ MeV, $\theta=50^\circ$) in the excitation energy region between 3.0 and 4.8 MeV.

IV. DATA REDUCTION

The data were replayed off line in order to optimize focal plane parameters. Cross sections were extracted from the experimental spectra using the line-shape fitted code ALLFIT [24]. The peak integrals extracted from the spectra via ALLFIT are corrected for Schwinger radiation, bremsstrahlung, and Landau straggling radiative effects as described by Bergstrom [25].

Several corrections were applied to the data in extracting cross sections. A deadtime correction, accounting for events not processed by the data acquisition system due to high count rates, was applied uniformly to each spectrum. Care was exercised during the data acquisition to constrain the count rate, either by lowering the beam current or decreasing the solid angle, to keep the deadtime correction to a few percent. A correction was also calculated during the analysis of the data to account for good events corrupted by intruder background events. Corrections for the finite acceptance of the spectrometer and multiple scattering from the target were also included in the analysis.

The raw cross sections were normalized to well-known levels in ^{208}Pb . The need for normalization arose from uncertainties and nonuniformities in the target thickness. These effects were corrected by an overall normalization applied to each data point. Using the Fourier-Bessel coefficients from a comprehensive analysis of previous electron scattering data on ^{208}Pb [26], electron scattering cross sections from the elastic level, and several of the well-determined inelastic levels (3^- , 2.615 MeV; 2^+ , 4.085 MeV; 4^+ , 4.323 MeV; 6^+ , 4.424 MeV; 8^+ , 4.610 MeV), were calculated at the appropriate kinematics.

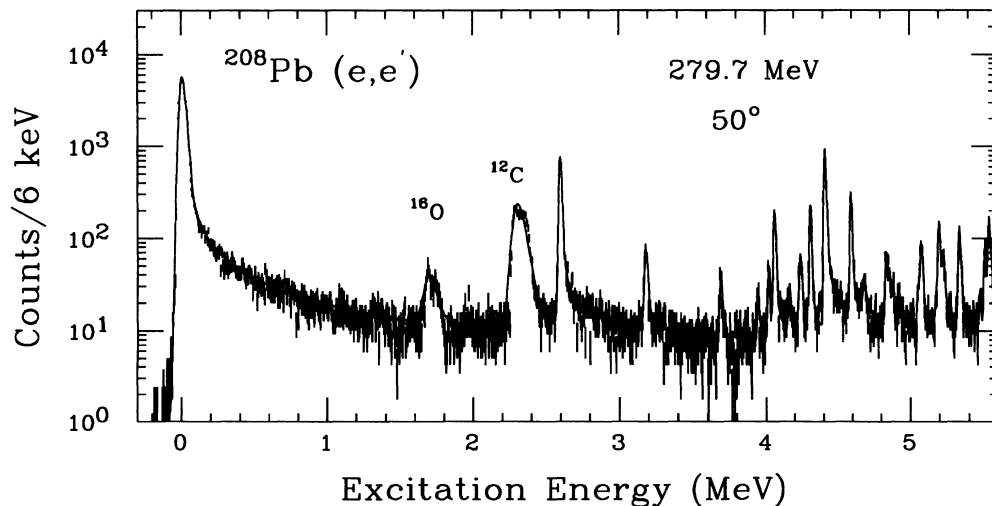


FIG. 1. Electron scattering measurements from ^{208}Pb . The momentum resolution is $5 \times 10^{-5} \Delta p/p$.

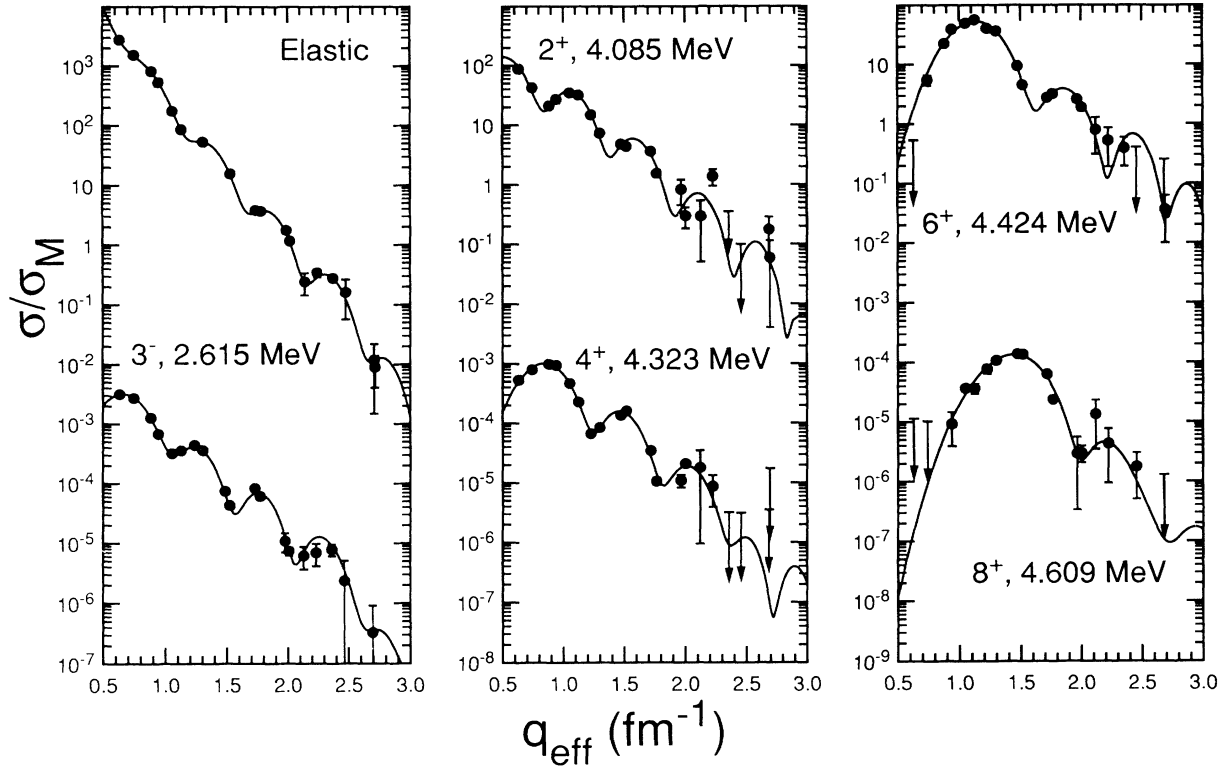


FIG. 2. Comparison of normalized cross sections to known form factors from Ref. [26].

The ratio of the calculated cross section to the raw unfolded experimental cross section was determined for each of the levels used in normalization. Normalizations extracted from different levels were consistent within the statistical accuracy. An overall normalization for each of the kinematics was obtained by a least-squares fit of a constant to the set of $(d\sigma/d\Omega_{\text{calc}})/(d\sigma/d\Omega_{\text{exp}})$. A comparison of the normalized data from this experiment to the known form factors is shown in Fig. 2.

The level density in ^{208}Pb is such that a separation of many levels is quite difficult even with a resolution of 20 keV. In order to determine the energies and extract cross sections for these transitions, the following method was employed. First, since the resolution of the forward angle data were generally better than the 155° data and the magnetic states contribute much less at forward angle, energies of peaks in the forward angle spectra were determined. Next, the backward angle data were fit, determining the energies of peaks at the momentum transfer where each level was at a maximum. The entire data set was then refit, using a consistent minimum set of energies required to give a good χ^2 . This method is dependent upon using a precise channel to energy calibration in the peak fitting routine. Consistency was therefore required in the energies of well-separated levels such as the 14^- at 6.745 MeV and the 6^+ at 5.997 MeV.

The major sources of uncertainty are the statistical errors, relative fitting errors (dependent upon correlations between each fitted peak and the background), and the uncertainty in the normalization. These errors were add-

ed in quadrature and applied to the final cross sections before the DWBA analysis were performed.

V. RESULTS

The highest spin states in ^{208}Pb were previously identified by Ref. [2] as 14^- at 6.74 MeV, 12^- at 6.37 MeV, and 12^- at 7.06 MeV. The $M14$ transition and lower $M12$ transition are due to the $(\nu 1j_{15/2}, 1i_{13/2}^{-1})$ 1p-1h excitation; the higher $M12$ transition is built upon the $\pi(1i_{13/2}, 1h_{11/2}^{-1})$ 1p-1h excitation. A purely transverse 12^+ level at 6.10 MeV was reported by Ref. [3] from the $\nu(1i_{11/2}, 1i_{13/2}^{-1})$ 1p-1h excitation. In those measurements, a 50% reduction from the single particle amplitude was determined for all four transitions.

Except for the 10^+ level at 5.92 MeV, no levels with spins and parities corresponding to those of the lower members of these multiplets have been previously identified. Although Tamm-Dankoff approximation (TDA) calculations [27] for the very high spin negative-parity electric states ($13^-, 11^-$) indicate that the electromagnetic cross section for these states is smaller than can be measured in this experiment, the large transverse cross section seen in electron scattering data in the group of levels near 5.8, 6.2, and 6.8 MeV at high momentum transfer suggest that at least the unnatural parity members of these multiplets have an appreciable cross section. The single particle energies of 5.85 MeV for the $\nu(1i_{11/2}, 1i_{13/2}^{-1})$ configuration, 6.49 MeV for the $\nu(1j_{15/2}, 1i_{13/2}^{-1})$ configuration, and 6.78 MeV for the

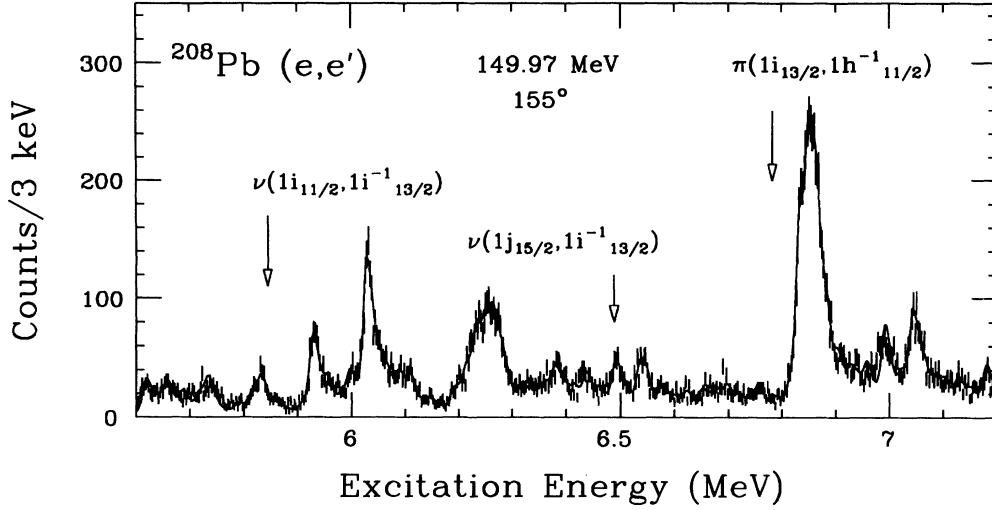


FIG. 3. Backward angle electron scattering spectrum ($q_{\text{eff}} \sim 1.5 \text{ fm}^{-1}$). Arrows indicate the energies of the 1p-1h configurations that couple to high spin states.

$\pi(1i_{13/2}, 1h_{11/2}^{-1})$ configuration reinforce this supposition. Figure 3 shows a fitted spectrum (155° , $E_0 = 149.9 \text{ MeV}$) of the excitation energy region between 5.8 and 7.2 MeV. Several multiplets are seen close to the predicted single particle energies.

The criterion used in the identification of states was threefold: (1) the matching of the q dependence of the form factor to that given by WS single particle predictions, (2) that the observed experimental excitation energies are close to the particle-hole energies, and (3) the absence of the longitudinal component to the form factor for magnetic or purely neutron transitions. Table I lists the levels seen in this experiment, the assigned multipolarity, and the dominant single particle configuration. The fitted normalization factors, indicating the degree of

quenching (zero quenching of the 1p-1h WS wave function give $N_q = 1$), are also listed in Table I.

A. 14^- , 12^- , and 12^+ levels

Our data for the $M14$ (6.745 MeV), $M12$ (6.347 MeV), and $E12$ (6.110 MeV) transitions agree with the measurements from Refs. [2,3]. Only the results from the DWBA fits will be presented for these levels.

As a pure 1p-1h excitation, the $M14$ transition can only proceed through the neutron $\nu(1j_{15/2}, 1i_{13/2}^{-1})$ excitation. This level dominates the high- q backward angle spectra ($q \geq 2.0 \text{ MeV}$) and displays no longitudinal component in the form factor. This aspect is displayed graphically in Fig. 4 by plotting the cross section divided

TABLE I. High spin transitions seen in this experiment with the dominant 1p-1h configuration and the normalization factor (N_q) of the Woods-Saxon DWBA fits to the data. An asterisk indicates the assignment of J^π is from this experiment.

Energy (MeV)	J^π	1p-1h configuration	N_q
5.010	9^+	$\nu(2g_{9/2}, 1i_{13/2}^{-1})$	0.54 ± 0.01
5.260	9^{+*}	$\pi(1h_{9/2}, 1h_{11/2}^{-1})$	0.53 ± 0.04
5.291	11^{+*}	$\nu(2g_{9/2}, 1i_{13/2}^{-1})$	0.38 ± 0.03
5.860	11^{+*}	$\nu(1i_{11/2}, 1i_{13/2}^{-1})$	0.61 ± 0.05
5.954	9^{+*}	$\nu(1i_{11/2}, 1i_{13/2}^{-1})$	0.50 ± 0.05
		$\pi(2f_{7/2}, 1h_{11/2}^{-1})$	0.19 ± 0.03
6.110	12^+	$\nu(1i_{11/2}, 1i_{13/2}^{-1})$	0.39 ± 0.06
6.283	10^{-*}	$\nu(1j_{15/2}, 1i_{13/2}^{-1})$	0.64 ± 0.07
6.437	12^-	$\nu(1j_{15/2}, 1i_{13/2}^{-1})$	0.46 ± 0.07
6.745	14^-	$\nu(1j_{15/2}, 1i_{13/2}^{-1})$	0.53 ± 0.04
6.833	$(8^-)^*$	$\pi(1i_{13/2}, 1h_{11/2}^{-1})$	0.58 ± 0.05
6.859	9^{-*}	$\pi(1i_{13/2}, 1h_{11/2}^{-1})$	0.55 ± 0.02
6.879	7^{-*}	$\pi(1i_{13/2}, 1h_{11/2}^{-1})$	0.39 ± 0.01
6.884	10^{-*}	$\pi(1i_{13/2}, 1h_{11/2}^{-1})$	0.32 ± 0.09
7.064	12^-	$\pi(1i_{13/2}, 1h_{11/2}^{-1})$	0.32 ± 0.05
7.086	12^{-*}	$\pi(1i_{13/2}, 1h_{11/2}^{-1})$	0.18 ± 0.02

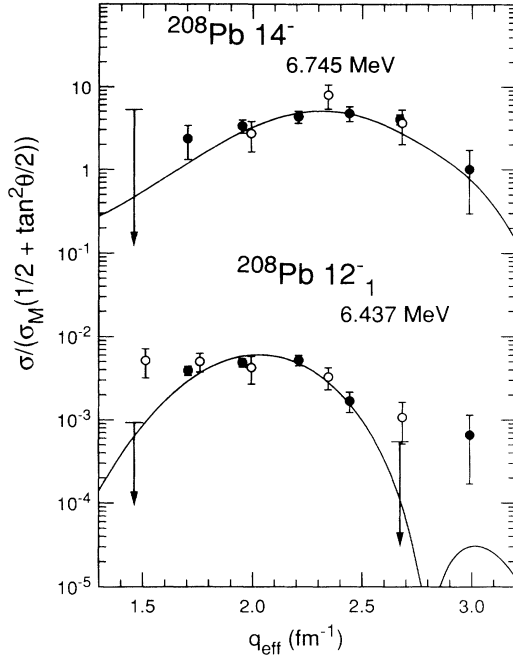


FIG. 4. $M14$ (6.745 MeV) and $M12$ (6.347 MeV) form factors with DWBA Woods-Saxon fits. The 6.745 MeV form factor is scaled by 1000. Forward angle data are represented by the open data points; the 155° data are presented by the solid data points.

by $\sigma_{\text{Mott}}[\frac{1}{2} + \tan^2(\theta/2)]$ vs q_{eff} . Any longitudinal component would enhance the forward angle data in this representation. The well radii of the WS single particle wave functions and the amplitude of the configuration were adjusted. We observed $52 \pm 4\%$ of the calculated single particle strength, slightly greater than the previously reported strength [2,4]. The fitted well radius was 1.225 ± 0.007 fm. This value is lower than the value reported by Ref. [2] (1.255 ± 0.003 fm) but closer to the well radius of 1.200 fm reported by Ref. [6] in a combined analysis of electron and proton scattering data.

The lower $M12$ transition is due primarily to the $\nu(1j_{15/2}, 1i_{13/2}^{-1})$ configuration. We obtain a reduction of the $1p$ - $1h$ transition to $46 \pm 7\%$ of the single particle strength. The WS fit to the form factor is shown in Fig. 4.

An $E12$ transition was observed at 6.110 ± 0.006 MeV in our experiment, 10 keV higher than reported by Ref. [3]. One expects this transition, a pure $1p$ - $1h$ neutron $\nu(1i_{11/2}, 1i_{13/2}^{-1})$ excitation, to be completely transverse; any longitudinal component measured will indicate the amount of effective charge produced by high-lying proton particle-hole components or $2p$ - $2h$ contributions to the $E12$ charge form factor.

The fit to the data, shown in Fig. 5, was performed varying both the WS radius and amplitude of the excitation. An effective magnetic moment of $g_{\text{eff}} = 0.627g_{\text{free}}$ was observed producing a reduction to $39 \pm 6\%$ of the single particle-hole strength, slightly lower than the $42 \pm 3\%$ quenching reported by Ref. [3]. The WS radius was 1.274 ± 0.03 fm. A comparison of forward and backward angle measurements confirms the conclusion by

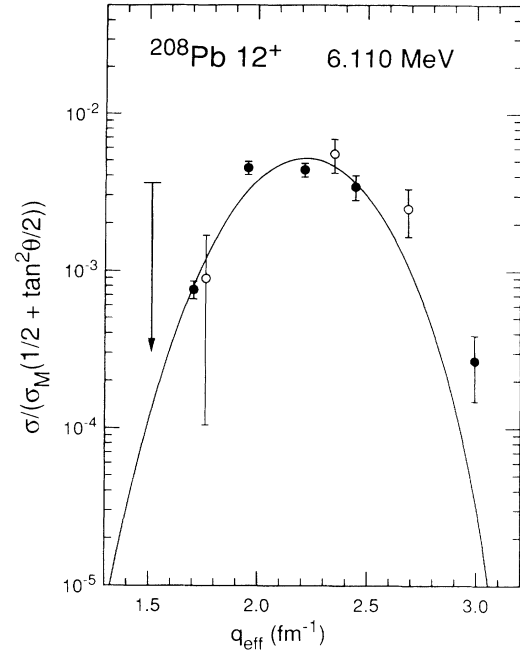


FIG. 5. $E12$ (6.110 MeV) form factor with DWBA Woods-Saxon fit. Forward angle data are represented by the open data points; the 155° data are represented by the solid data points.

Ref. [3] that no measurable longitudinal strength is seen in the 12^+ cross section.

The higher $M12$ transition at 7.06 MeV was reported [2] as due to the proton $\pi(1i_{13/2}, 1h_{11/2}^{-1})$ excitation. In our experiment, the increased resolution permitted the separation of two levels, not resolved in the previous experiment, at 7.064 and 7.086 MeV. Figure 6 displays the excitation energy region between 6.9 and 7.2 MeV at $E_i = 201$ MeV and $\theta = 155^\circ$. A level at 7.086 MeV is observed close to the stronger known 12^- level at 7.064 MeV. This level appears to be transverse and peaks at a momentum transfer of $q_{\text{eff}} = 2.1$ fm $^{-1}$. In Fig. 7(a), a comparison is made between the backward angle cross sections for the 7.064 MeV 12^- state and the 7.086 MeV level. The form factors are nearly identical in shape although the level at 7.086 MeV displays less strength than the 7.064 MeV state. Also shown are the fitted curves to the data, assuming both transitions are $\pi(1i_{13/2}, 1h_{11/2}^{-1})_{12^-}$ excitations.

In Fig. 7(b), the sum of our data for the 7.064 and 7.086 MeV levels are shown with the DWBA fit obtained by Ref. [2] from their fit to the reported $M12$ transition at 7.06 MeV. The sum reproduces the cross section reported by Ref. [2], suggesting that both states were included in the previous (e, e') analysis of the $M12$ transition at 7.06 MeV. The similarity between the shapes of the form factors for these two levels and the lack of longitudinal strength renders these levels difficult to resolve for energy resolutions worse than 25 keV.

Initially, we fit the 7.086 MeV form factor as an $M10$ transition. The only configuration providing enough strength at large momentum transfer to give a reasonable χ^2 was the $\nu(1i_{11/2}, 1h_{9/2}^{-1})$ with a single particle-hole en-

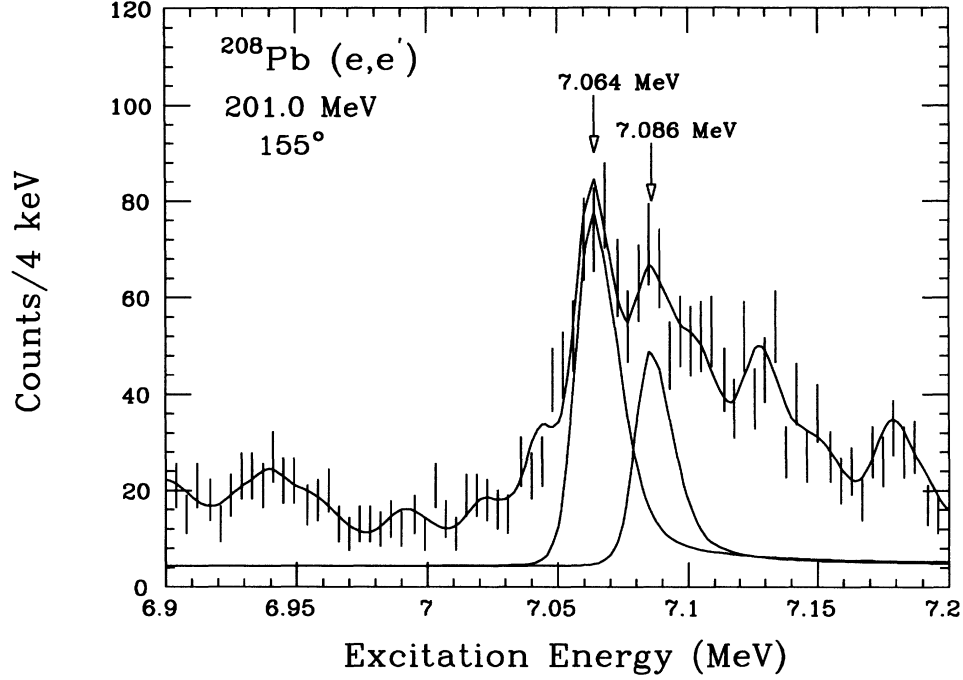


FIG. 6. Backward angle electron scattering spectrum ($q_{\text{eff}} \sim 2.0 \text{ fm}^{-1}$) between 6.9 and 7.2 MeV.

ergy of 7.62 MeV. It is unlikely that the experimental energy would be lowered by almost 600 keV unless strong mixing occurred. This is not expected for magnetic transitions. A more likely possibility is the fragmentation of the 12^- strength through mixing with a two-phonon configuration.

Both transitions were analyzed assuming a pure $\pi(1i_{13/2}, 1h_{11/2}^{-1})$ WS configuration for both the 7.064 and 7.086 MeV levels [Fig. 7(a)]. The strength of the proton $1p-1h$ $M12$ transition at 7.064 MeV was $32 \pm 5\%$ of the calculated single particle prediction. The fitted single particle radius was $1.288 \pm 0.007 \text{ fm}$. Identifying the peak

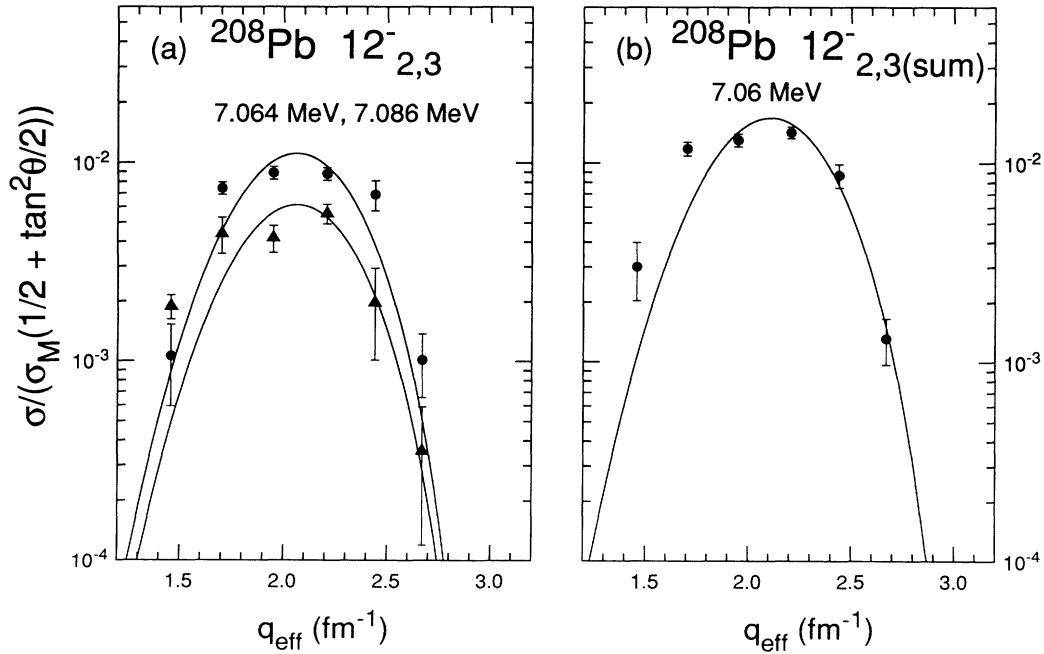


FIG. 7. (a) Form factors of the 7.064 MeV (circles) and 7.086 MeV (triangles) levels. Fits assume an $M12$ $\pi(1i_{13/2}, 1h_{11/2}^{-1})_{12^-}$ $1p-1h$ excitation for both levels. (b) Sums of 7.064 and 7.086 MeV form factors compared to the fit of the 7.06 MeV $M12$ transition from Ref. [2]. All data were taken at a scattering angle of 155° .

at 7.086 MeV as a 12^- level, the state carries $18 \pm 2\%$ of the single particle strength.

As a consistency check, the summed cross sections from 7.064 MeV and 7.086 levels were fit. The combined strength from this analysis was $53 \pm 3\%$ of the $\pi(1i_{13/2}, 1h_{11/2}^{-1})$ transition. This reproduces the result from Ref. [2] of a 50% reduction of the 1p-1h form factor.

This small splitting suggests a different coupling mechanism at work than that proposed by Daheza, Speth, and Faessler [28] of particle-phonon coupling. Instead, this seems to indicate one-phonon–two-phonon coupling. It implies that a two-phonon state is almost degenerate in energy with the 12^- one-phonon excitation. A very small coupling constant can cause a splitting of 22 keV and significant mixing such that one state carries $\frac{1}{3}$ of the strength and the other carries $\frac{2}{3}$ of the strength.

A possible candidate for such a two-phonon configuration is the $(3^- \otimes 10^+)_{12^-}$, where the phonon-phonon self-energy reduces the energy of this configuration from the sum of the two-phonon energies of (2.615 + 4.89) MeV. Calculations to test this hypothesis are underway. In any case, the small splitting indicates that the coupling of the 12^- excitation with the two-phonon state is rather small.

B. 11^+ levels

Only two configurations with a single particle energy below 7.2 MeV can couple to $M11$ transitions: the $\nu(2g_{9/2}, 1i_{13/2}^{-1})$ with a single particle energy of 5.067 MeV, and the $\nu(1i_{11/2}, 1i_{13/2}^{-1})$ with a single particle energy of 5.845 MeV. The only indication of possible $M11$ transition strength in ^{208}Pb in previous measurements was a tentative assignment of $J^\pi = 11^+$ to a level seen at 5.27 MeV in an (e, e') measurement [29].

We assign $J^\pi = 11^+$ to levels seen at 5.291 and 5.860 MeV. The fits to the form factor were analyzed assuming no mixing of the two possible 11^+ configurations. One would expect very little configuration mixing due to the large gap between the single particle energies and the slightly repulsive residual interaction for magnetic transitions. However, as shown by Ref. [1], configuration mixing between the 12^- configurations may be responsible for the differences seen between electron and proton scattering in the $M12$ form factors. Unfortunately, the sensitivity to small amounts of configuration mixing in this experiment is limited by the number of data points (7) at backward scattering angles.

The fits to the data are shown in Fig. 8. The analysis was performed by adjusting only the amplitudes of the WS configurations. The WS orbital radii were determined by the fits to strongly excited levels based upon the same configuration; the radii of the $\nu(2g_{9/2}, 1i_{13/2}^{-1})$ wave functions were taken from the fit to the $E10$ transition at 5.072 MeV and the radii of the $\nu(1i_{11/2}, 1i_{13/2}^{-1})$ wave functions were taken from the fit to the transition at 6.110 MeV. The analysis shows a reduction of the calculated 1p-1h strength in both transitions: $22 \pm 9\%$ of the $\nu(2g_{9/2}, 1i_{13/2}^{-1})$ strength in the 5.291 MeV $M11$ transition and $61 \pm 5\%$ of the $\nu(1i_{11/2}, 1i_{13/2}^{-1})$ strength in the 5.860

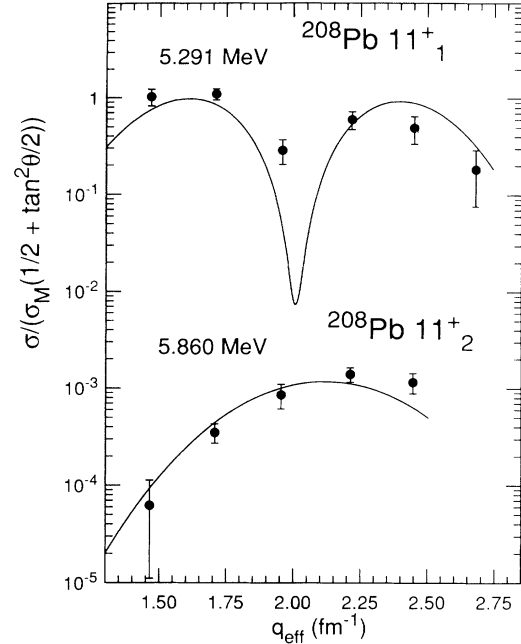


FIG. 8. Form factors for the $M11$ transitions at 5.291 and 5.860 MeV with DWBA Woods-Saxon fits. The 5.291 MeV form factor is scaled by 1000. All data were taken at a scattering angle of 155° .

MeV $M11$ transition.

The momentum transfer dependence of the two 11^+ form factors are much different from one another. The $\nu(1i_{11/2}, 1i_{13/2}^{-1})$ 1p-1h excitation produces a form factor shape characterized by a broad peak in momentum space. The 5.291 MeV form factor, however, has a minimum near 2.0 fm^{-1} . This feature is due to a change in the radial quantum numbers from $n=1 \rightarrow n=2$ in the contributing wave functions of the $\nu(2g_{9/2}, 1i_{13/2}^{-1})$ configuration. This case provides a clear example of the sensitivity of electron scattering to the microscopic structure of nuclear transitions.

C. 10^- levels

The only two configurations coupling to 10^- with a single particle energy below 7.2 MeV are the $\nu(1j_{15/2}, 1i_{13/2}^{-1})$ and $\pi(1i_{13/2}, 1h_{11/2}^{-1})$ 1p-1h excitations. A search for $M10$ transitions was made in the multiplet of levels near 6.2 and 6.8 MeV.

A group of closely spaced levels near 6.2 MeV excitation energy are likely to be members of the multiplet based upon the $\nu(1j_{15/2}, 1i_{13/2}^{-1})$ configuration. Several negative-parity states ($3^-, 5^-, 7^-$) have been reported in this region [30]. As seen in Fig. 3, the level density is very high in this energy region. Only one form factor has been reliably extracted from this multiplet. A level at 6.283 MeV peaks at higher momentum transfer than other levels seen in this multiplet. The forward angle cross section of the 6.283 MeV level was small and was obscured by the longitudinal strength of neighboring levels.

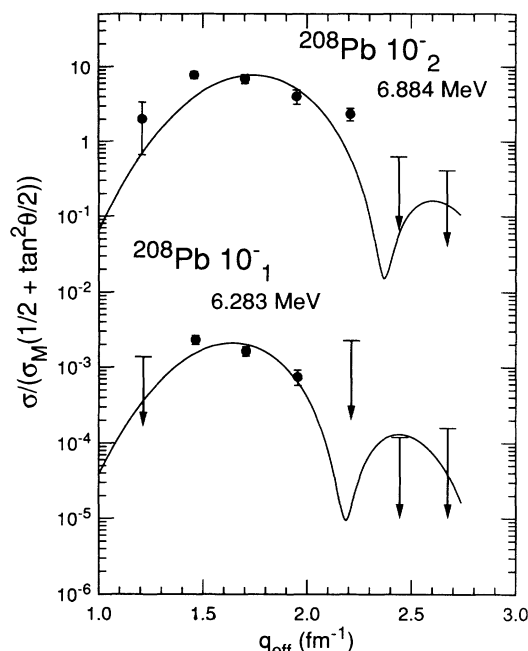


FIG. 9. Form factors for the $M10$ transitions at 6.283 and 6.884 MeV with DWBA Woods-Saxon fits. The 6.884 MeV form factor is scaled by 1000. All data were taken at a scattering angle of 155° .

The lack of a measurable strength at forward angles suggests that the excitation is dominantly transverse. An assignment of 10^- was made to the 6.283 MeV excitation based upon the shape of the form factor and the strength of the excitation. The predicted form factor shape of the $M8$ transition from the $\nu(1j_{15/2}, 1i_{13/2}^-)$ configuration peaks at 1.2 fm^{-1} and gave a poor fit to the data.

In the DWBA analysis, two one-phonon WS configurations were included in the fit, the $\nu(1j_{15/2}, 1i_{13/2}^-)$ and $\pi(1i_{13/2}, 1h_{11/2}^-)$ using the radial parameters obtained from the analysis of the 12^- levels at 6.437 and 7.064 MeV. The best fit was obtained with the excitation being $64 \pm 7\%$ of the $\nu(1j_{15/2}, 1i_{13/2}^-)$ transition and $2 \pm 1\%$ of the $\pi(1i_{13/2}, 1h_{11/2}^-)$ transition.

In the search for magnetic transitions in the 6.85 MeV multiplet, only one level fulfilled the criteria established to justify an assignment of spin and parity. A level at 6.884 MeV was analyzed as an $M10$ transition based upon the $\pi(1i_{13/2}, 1h_{11/2}^-)$ configuration. A reduction to $32 \pm 9\%$ of the predicted WS transition strength was seen. The form factors for the 6.283 and 6.884 MeV transitions are shown in Fig. 9.

D. 7^- and 9^- levels

The multiplet of states near 6.85 MeV display large cross sections in the momentum transfer region between 1.2 and 2.0 fm^{-1} in both the forward and backward angle data. These levels are quite close to the effective single particle-hole energy (6.75 MeV) of the $\pi(1i_{13/2}, 1h_{11/2}^-)$ configuration.

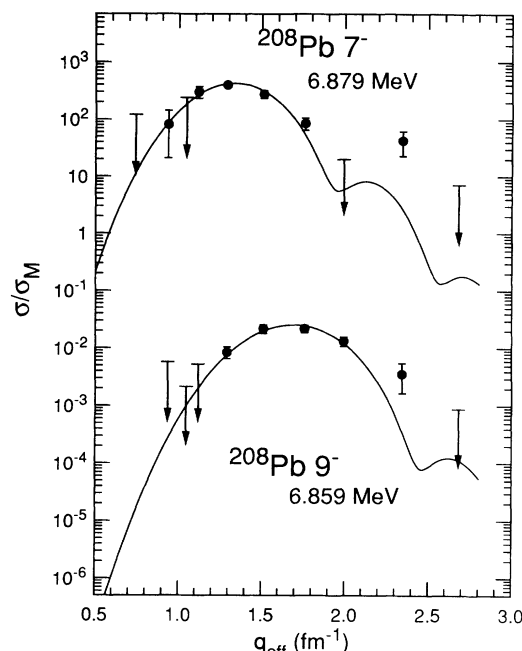


FIG. 10. Forward angle data for the 6.879 MeV 7^- level and the 6.859 MeV 9^- level. Fits were performed assuming purely longitudinal transitions. The 6.879 MeV form factor is scaled by 1000. The data are from the forward angle measurements only.

Two strong transitions at 6.859 and 6.879 MeV were seen in the forward angle spectra with apparently strong longitudinal components. We identify these levels as 9^- (6.859 MeV) and 7^- (6.879 MeV). TDA calculations [27] indicate that both transitions have a very small transition current density. For this reason, the 6.879 and 6.859 MeV levels were fit only in the forward angle data and analyzed assuming a purely longitudinal transition. The DWBA analysis was performed assuming a pure $\pi(1i_{13/2}, 1h_{11/2}^-)$ 1p-1h excitation; the radius was held fixed at the value obtained from the analysis of the 12^- level at 7.064 MeV and the amplitude was allowed to vary. The fits to the data are displayed in Fig. 10. The experimental form factor was found to contain $39 \pm 1\%$ of the predicted 1p-1h strength for the $E7$ transition, and $55 \pm 2\%$ of the predicted 1p-1h strength for the $E9$ transition.

E. 9^+ levels

In the excitation energy region below 7.2 MeV, we identify three levels with a possible spin and parity of 9^+ : 5.010, 5.260, and 5.954 MeV. Only levels reported at 5.01 and 7.00 MeV have been previously identified as $M9$ transitions [29]. We confirm the assignment of 9^+ to the level at 5.01 MeV; no evidence was seen in this experiment for an identification of 9^+ to levels near 7.00 MeV.

There are five configurations with a single particle energy between 5.0 and 6.0 MeV that couple to 9^+ . Configuration mixing may be significant if 1p-1h energies are close. TDA calculations [27], however, predict very

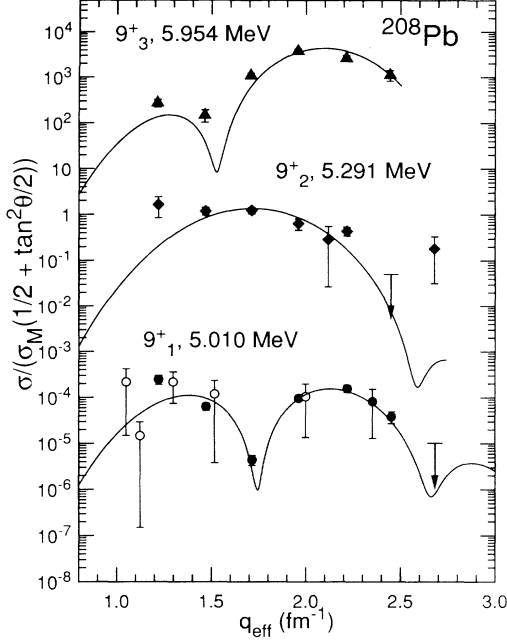


FIG. 11. Form factors for the $M9$ transition at 5.010, 5.291 ($\times 10^3$), and 5.954 MeV ($\times 10^6$) with DWBA Woods-Saxon fits. Forward angle data are represented by open data points; the solid data points were taken at 155° scattering angle.

little mixing between the $\pi(1h_{9/2}, 1h_{11/2}^{-1})$ and $\nu(2g_{9/2}, 1i_{13/2}^{-1})$ configurations in the two lowest $M9$ transitions.

Form factors from the $M9$ transition at 5.010 and 5.260, and 5.954 MeV were fit with WS wave functions from the two configurations with single particle energies closest to that of the observed level. In the analysis of the 5.010 and 5.260 MeV levels, a single 1p-1h excitation dominated the fit; the amplitude of the second configuration in both cases were fitted to zero within the uncertainties. We obtained a good fit for the 5.010 MeV $M9$ form factor from the $\nu(2g_{9/2}, 1i_{13/2}^{-1})$ excitation scaled by 54.0%. The level at 5.260 MeV is dominated by the proton spin-flip transition $\pi(1h_{9/2}, 1h_{11/2}^{-1})$ reduced to 52.7% of the 1p-1h strength. The analysis of the 5.954 MeV 9^+ level gave mixing percentages of 0.50 ± 0.05 for the $\nu(1i_{11/2}, 1i_{13/2}^{-1})$ configuration and 0.19 ± 0.03 for the $\pi(2f_{7/2}, 1h_{11/2}^{-1})$ configuration. The fitted form factors are shown in Fig. 11.

F. 8^- levels

Six one-phonon configurations with a single particle energy less than 7.0 MeV couple to 8^- in ^{208}Pb . However, we were only able to identify the level at 6.833 MeV as a candidate for an $M8$ transition. This level is part of the multiplet of states resulting from the $\pi(1i_{13/2}, 1h_{11/2}^{-1})$ excitation.

Although one would expect an $M8$ transition near this excitation energy, our assignment must be considered tentative, due primarily to the quality of the DWBA fit. The analysis was performed assuming a pure

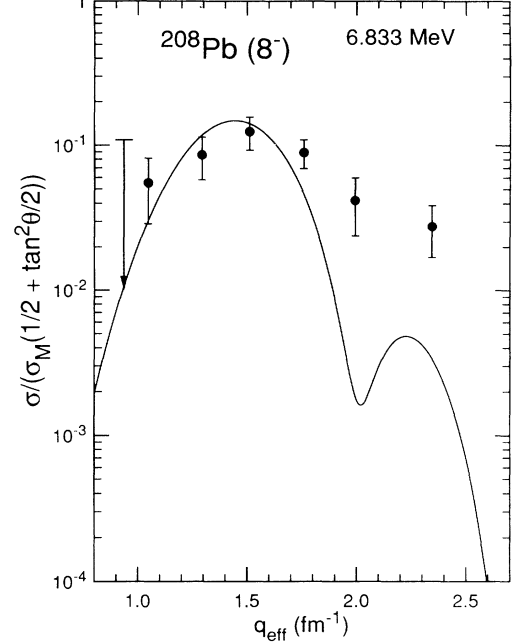


FIG. 12. Form factor for the transition seen at 6.833 MeV. The level is tentatively identified as an $M8$ transition. The solid line represents the DWBA Woods-Saxon fit.

$\pi(1i_{13/2}, 1h_{11/2}^{-1})$ transition. The fitted strength of the one-phonon transition was $58 \pm 5\%$ of the pure WS excitation. The form factor is plotted in Fig. 12, along with the results from the analysis.

The high momentum transfer behavior of the 6.833 MeV does not agree with the calculated shape of the form factor based upon a pure $\pi(1i_{13/2}, 1h_{11/2}^{-1})$ phonon. Although the maxima of the form factors coincide, the data do not warrant a strong identification of 8^- to this level.

VI. CONCLUSIONS

At high momentum transfer, the excitation energy region in ^{208}Pb above 5.0 MeV is populated by levels resulting from the $\nu(1i_{11/2}, 1i_{13/2}^{-1})$, $\pi(1i_{13/2}, 1h_{11/2}^{-1})$, $\nu(2g_{9/2}, 1i_{13/2}^{-1})$, and $\nu(1j_{15/2}, 1i_{13/2}^{-1})$ configurations. Although the highest multipolarity states have been identified and studied in earlier experiments, the lower spin states, except for the 10^+ levels [3], have not been previously reported. Assignments of J^π have been made to several electric and magnetic excitations, and have been analyzed in terms of WS single particle-hole wave functions. Reductions of 22–65 % from calculated single particle-hole strengths are seen in 9^+ , 10^- , and 11^+ excitations.

Our measurements on the very high spin states (14^- , 12^- , 12^+) agree with the measurements made by Ref. [2] except for the 7.06 MeV 12^- level which our experiment identified as a doublet unresolved in previous electron scattering experiments. The sum of the cross section from the 7.068 and 7.086 MeV levels agree with the 7.06 MeV 12^- level cross section reported in Ref. [2]. The observed strength of the 7.068 MeV state was only

$32 \pm 5\%$ of the single particle-hole strength. The fragmentation of the proton $M12$ transition is interpreted as evidence of a two-phonon excitation near 7.1 MeV. This is the first time that fragmentation of such a high spin state has been observed, and as such may shed some light on the relative importance of the two competing quenching mechanisms, namely, fragmentation of strength and reduction of strength due to partial occupancy.

A remarkable feature of Table I is the substantial reduction in single particle strength in all 15 transitions. The highest strength observed is 0.64 ± 0.09 (for the $M10$ transition at 6.283 MeV) and the lowest is 0.32 ± 0.09 (for the $M10$ transition at 6.884 MeV). For multipolarities of the highest spin (12,14), where mixing and fractionation is minimal and better understood, we observe a more narrow range of values, values very close to 0.5.

Of the various mechanisms that have been proposed to explain the reduction ("quenching") of spectroscopic strength of high spin states in the lead region, only the fractional occupancy of the shell-model orbitals appears to provide a consistent explanation of our data and other related phenomena in these nuclear systems. In many cases, as shown in Ref. [8], the effect of core polarization is compensated by meson exchange contributions and the resulting reduction in spectroscopic strength is much smaller than the observed one. An example of the inadequacy of core polarization alone to account for the universal reduction observed can be found in the case of the $E9$ (6.859 MeV) longitudinal form factor from the $1p$ - $1h$ amplitude of the $\pi(1i_{13/2}, 1h_{11/2}^{-1})$ excitation, where such models predict minimal quenching. Quenching resulting from $2p$ - $2h$ contributions are not expected to be adequate to produce the observed large reduction, al-

though they constitute one of the many mechanisms that produce fractional occupancy. As such, $2p$ - $2h$ quenching is included in the more general explanation offered by fractional occupancy.

Estimates of the expected quenching resulting from fractional occupancy and consistent with the measured Z factors of the neutron and proton shells [31] range between 0.4 and 0.7. In addition to this underlying many-body mechanism, the influence of effects such as core polarization and meson exchange current contributions is expected to bring fluctuations to the measured quenching factors in any given excitation. Such calculations for most of the states examined are not available; their need is apparent. However, the overall consistency of quenching observed in our experiment for such an extensive number of excitations (both electric and magnetic) strongly supports the assertion that fractional occupancy of shell-model orbits is primarily responsible for the lack of strength in single particle transitions throughout the Periodic Table.

ACKNOWLEDGMENTS

We acknowledge the directors, staff, and scientists at the William F. Bates Linear Electron Accelerator Center for their support throughout this experiment. We also thank Steve Dolfini and Joe Mandeville of the University of Illinois for their assistance in the data acquisition. This work has been supported in part by Department of Energy Contract No. DE-FG02-88ER40410 and by the National Science Foundation under Grant No. NSF PHY 89-21146.

-
- [1] A. M. Lallena, Nucl. Phys. **A489**, 70 (1988).
 - [2] J. Lichtenstadt, J. Heisenberg, C. Papanicolas, C. Sargent, A. Courtemanche, and J. S. McCarthy, Phys. Rev. C **20**, 497 (1979).
 - [3] J. Lichtenstadt, C. N. Papanicolas, C. Sargent, J. Heisenberg, and J. McCarthy, Phys. Rev. Lett. **44**, 858 (1980).
 - [4] A. D. Bacher, G. T. Emery, W. P. Jones, D. W. Miller, G. S. Adams, F. Petrovich, and W. G. Love, Phys. Lett. **97B**, 58 (1980).
 - [5] G. S. Adams, A. D. Bacher, G. T. Emery, W. P. Jones, D. W. Miller, F. Petrovich, and W. G. Love, Phys. Lett. **91B**, 23 (1980).
 - [6] D. Cook, N. M. Hintz, M. Gazzaly, G. Pauletta, R. W. Ferguson, G. W. Hoffman, J. B. McClelland, and K. W. Jones, Phys. Rev. C **35**, 456 (1987).
 - [7] I. Hamamoto, J. Lichtenstadt, and G. F. Bertsch, Phys. Lett. **93B**, 213 (1980).
 - [8] T. Suzuki, M. Oka, H. Hyuga, and A. Arima, Phys. Rev. C **26**, 750 (1982).
 - [9] S. Krewald and J. Speth, Phys. Rev. Lett. **45**, 417 (1980).
 - [10] V. R. Pandharipande, C. N. Papanicolas, and J. Wambach, Phys. Rev. Lett. **53**, 1133 (1984).
 - [11] C. N. Papanicolas, *Nuclear Structure at High Spin Excitation and Momentum Transfer (McCormick's Creek State Park, Bloomington, Indiana)*, Proceedings of the Workshop on Nuclear Structure at High Spin, Excitation, and Momentum Transfer, AIP Conf. Proc. No. 142, edited by Hermann Nann (AIP, New York, 1985).
 - [12] C. N. Papanicolas and S. E. Williamson, Inst. Phys. Conf. Ser. **105**, 197 (1990).
 - [13] T. deForest and J. D. Walecka, Adv. Phys. **15**, 1 (1966).
 - [14] H. Überall, *Electron Scattering from Complex Nuclei* (Academic, New York, 1971).
 - [15] J. D. Walecka, NTIS Report ANL-83-50, 1983.
 - [16] H. C. Lee, Atomic Energy of Canada Report AECL-4839, 1975.
 - [17] J. Heisenberg, Adv. Nucl. Phys. **12**, 61 (1981).
 - [18] FOUBES1, FOUBES2, and FOUBES2A, J. Heisenberg, unpublished.
 - [19] S. T. Tuan, L. E. Wright, and D. S. Onley, Nucl. Instrum. Methods **60**, 70 (1968).
 - [20] G. A. Rinker and J. Speth, Nucl. Phys. **A306**, 360 (1978).
 - [21] G. G. Simon, Ch. Schmitt, F. Borkowski, and V. H. Walther, Nucl. Phys. **A173**, 32 (1971).
 - [22] W. Bertozzi, M. V. Hynes, C. P. Sargent, W. Turchinets, and C. Williamson, Nucl. Instrum. Methods **162**, 211 (1979).
 - [23] W. Bertozzi, M. V. Hynes, C. P. Sargent, C. Cresswell, P.

- C. Dunn, A. Hirsh, M. Seitch, B. Norum, F. N. Rad, and T. Sasanuma, *Nucl. Instrum. Methods* **141**, 457 (1977).
- [24] J. J. Kelly, C. E. Hyde-Wright, and F. W. Hersman, ALLFIT computer code, unpublished.
- [25] J. Bergstrom, *MIT 1967 Summer Study, Medium Energy Nuclear Physics with Electron Accelerators* (MIT, Cambridge, Massachusetts, 1967), p. 251.
- [26] J. Heisenberg, J. Lichtenstadt, C. N. Papanicolas, and J. S. McCarthy, *Phys. Rev. C* **25**, 2292 (1982).
- [27] J. H. Heisenberg, unpublished.
- [28] J. S. Daheza, J. Speth, and A. Faessler, *Phys. Rev. Lett.* **38**, 208 (1977).
- [29] J. Lichtenstadt, Ph.D. thesis, MIT, 1979.
- [30] M. J. Martin, *Nucl. Data Sheets* **47**, 797 (1986).
- [31] C. N. Papanicolas, L. S. Cardman, J. H. Heisenberg, O. Schwenter, T. E. Milliman, F. W. Hersman, R. S. Hicks, G. A. Peterson, J. S. McCarthy, J. Wise, and B. Frois, *Phys. Rev. Lett.* **58**, 2296 (1987).